Received: 10 April 2021 | Revised: 5 April 2022 | Accepted: 1 June 2022

DOI: 10.1002/mp.15803

RESEARCH ARTICLE

MEDICAL PHYSICS

Artificial intelligence–based CT metrics used in predicting clinical outcome of COVID-19 in young and middle-aged adults

Yu Xudong[1] | **Liu Weihong**[2] | **Xia Feng**[1] | **Li Yanli**[3] | **Lan Weishun**[1] | **Zhang Fengjun**[4] | **Gao Jiao**[2] | **Li Jiawei**[2] | **Huang Xiaolu**[2] | **Huang Huailiang**[5] | **Liang Jianye**[6] | **Zeng Sihui**[6] | **Xie Chuanmiao**[6] | **Li Hanhui**[7] | **Mao Liang**[7]

[1]Department of Medical Imaging, Maternal and Child Health Hospital of Hubei Province, Wuhan, China

[2]Department of Radiology, General Hospital of China Resources & Wuhan Iron and Steel Corporation, Wuhan, China

[3]Department of Gynecology, Maternal and Child Health Hospital of Hubei Province, Wuhan, China

[4]Jiangsu Digital Medical Laboratory, Nanjing University of Aeronautics and Astronautics, Nanjing, China

[5]Medical College of Soochow University, Suzhou, Jiangsu, China

[6]Department of Medical Imaging, Sun Yat-sen University Cancer Center, State Key Laboratory of Oncology in South China, Guangzhou, China

[7]Department of Research and Development, Shanghai United Imaging Intelligence Co. Ltd., Shanghai, China

Correspondence
Yu Xudong, Department of Medical Imaging, Maternal and Child Health Hospital of Hubei Province, Wuhan 430070, China.
Email: 710527720@qq.com

Liu Weihong, Department of Radiology, General Hospital of China Resources & Wuhan Iron and Steel Corporation, Wuhan 430080, China.
Email: liuwhwygh@sina.com

Zhang Fengjun, Jiangsu Digital Medical Laboratory, Nanjing University of Aeronautics and Astronautics, Nanjing 210000, China.
Email: jszhfj@nuaa.edu.cn

Funding information
Financial/nonfinancial disclosures: No fund.

Abstract

Background: Currently, most researchers mainly analyzed coronavirus disease 2019 (COVID-19) pneumonia visually or qualitatively, probably somewhat time-consuming and not precise enough.

Purpose: This study aimed to excavate more information, such as differences in distribution, density, and severity of pneumonia lesions between males and females in a specific age group using artificial intelligence (AI)-based computed tomography (CT) metrics. Besides, these metrics were incorporated into a clinical regression model to predict the short-term outcome.

Materials and methods: The clinical, laboratory information and a series of HRCT images from 49 patients, aged from 20 to 50 years and confirmed with COVID-19, were collected. The volumes and percentages of infection (POIs) among bilateral lungs and each bronchopulmonary segment were extracted using uAI-Discover-NCP software (version R001). The POI in three HU ranges (i.e., <−300, −300–49, and ≥50 HU representing ground-glass opacity [GGO], mixed opacity, and consolidation) were also extracted. Hospital stay was predicted with several POI after adjusting days from illness onset to admission, leucocytes, lymphocytes, C-reactive protein, age, and gender using a multiple linear regression model. A total of 91 patients aged 20–50 from public database were selected.

Results: Right lower lobes had the highest POI, followed by left lower lobes, right upper lobes, middle lobes, and left upper lobes. The distributions in lung lobes and segments were different between the sexes. Men had a higher total POI and GGO of the lungs, but less consolidation than women in initial CT (all $p < 0.05$).

Abbreviations: AI, artificial intelligence; COVID-19, coronavirus disease 2019; CRP, C-reactive protein; CT, computed tomography; GGO, ground-glass opacity; POI, percentage of infection; RT-PCR, reverse transcription polymerase chain reaction; SARS-CoV-2, severe acute respiratory syndrome coronavirus 2.

The total POI, percentage of consolidation on initial CT, and changed POI were positively correlated with hospital stay in the model. A total of 91 patients aged 20–50 years in the public database were selected, and AI segmentation was performed. The POI of the lower lobes was obviously higher than that in the upper lobes; the POI of each segment of the right upper lobe in the males was higher than that in the females, which was consistent with the result of the 49 patients previously.

Conclusion: Both men and women had characteristic distributions in lung lobes and bronchopulmonary segments. AI-based CT quantitative metrics can provide more precise information regarding lesion distribution and severity to predict clinical outcome.

KEYWORDS

artificial intelligence, COVID-19, distribution, outcome, percentages of infection, quantitative metrics

1 | INTRODUCTION

Beginning in December 2019, a new pneumonia named coronavirus disease 2019 (COVID-19) was initially reported in Wuhan, Hubei province and has gradually spread throughout the country. COVID-19 has quickly spread worldwide, with more than 500 million people infected and resulting in over 6 million deaths. The confirmed number has exceeded 290 000 from other countries, with more than 15 000 deaths. As the World Health Organization announced the outbreak of COVID-19 as a Public Health Emergency of International Concern on 30 January 2020, many countries or regions have successively declared a state of emergency and upgraded their responses to the first/highest level. The disease was caused by a betacoronavirus, which was newly named severe acute respiratory syndrome coronavirus 2 (SARS-CoV-2). It has a strong infectivity from person to person. However, the clinical symptoms and disease severity varied a lot among different crowds, with an overall mortality of 2%.

Reverse transcription polymerase chain reaction (RT-PCR) or gene sequencing is the golden standard for the diagnosis of COVID-19. However, they have several limitations such as inadequate test kits for timely diagnosis in a large population suspected. Besides, the total positive rate was reported to be only 30%–60% at an initial test due to its low sensitivity.[1] In addition, false negatives because of low viral load and false positives caused by the presence of viral fragments in the respiratory tract after infection have also been found.[2] For the high acquisition speed and accuracy in detecting pulmonary lesions, computed tomography (CT) has been affirmed as the preferred imaging tool in diagnosing COVID-19 and recommended as the major evidence for clinically diagnosed cases in this epidemic in Hubei, China.[2] Currently, most researchers mainly analyzed COVID-19 pneumonia visually or qualitatively, which probably time-consuming and exhausting, especially in a rapidly increasing infected population and when demanded to compare with previous examinations.[3] The accuracy was low as a lot of information based on lesions volumes and density were omitted. Besides, the blurred lesion borders and low density of ground-glass opacity (GGO) will confuse radiologists when evaluating the lesion severity. Inspiringly, artificial intelligence (AI) based on deep learning technology has been attempted to diagnose COVID-19 and make a differentiation from other pneumonia, which demonstrates a great prospect for its high capability in feature extraction.[4,5] Shan et al.[6] employed the "VB-Net" neural network to segment COVID-19 infection and a human-in-the-loop strategy to train the system for quantification of infection regions. The system generated a Dice similarity coefficient as high as 90% between automatic and manual segmentations, and a mean percentage of infection (POI) estimation error of 0.3% for the whole lung on the validation dataset, which indicated a high accuracy for automatic infection region delineation.

The occurrence and case fatality rate was revealed higher in men in a similar viral pneumonia (MERS-CoV infection).[7] However, limited data were available about the difference between the sexes when comparing the epidemiological, clinical, and imaging feature in COVID-19. Hence we employed the deep learning system to extract quantitative CT metrics to compare the difference in distribution, density, and severity of pneumonia lesions between males and females in a specific age group, to maximally eliminate the influence of age, especially in children and the elderly. Besides, these metrics were incorporated into a clinical regression model to predict the short-term outcome.

2 | MATERIALS AND METHODS

2.1 | Patients

This study was conducted in accordance with the amended Declaration of Helsinki and had been approved by the ethics committee of General hospital of China Resources & Wuhan Iron and Steel Corporation

(IRB 20200345). The individual consent was waived due to the retrospective nature. The clinical, laboratory, and CT imaging data of patients with COVID-19 in General Hospital of China Resources & Wuhan Iron and Steel Corporation from 11 January 2020 to 18 March 2020 were collected and analyzed retrospectively. The inclusion criteria were as follows: (1) the patients were confirmed with SARS-CoV-2 by real-time fluorescent RT-PCR or viral gene sequence; (2) the patients aged from 20 to 50 years; (3) moderate, severe, and critical patients with radiological findings of pneumonia according to the Diagnosis and Treatment Protocol for Novel Coronavirus Pneumonia (Trial Version 7),[8] and (4) those who completed the initial chest CT examination within 3 days after the illness onset and had at least one follow-up CT scan within 1 week after the initial examination. The general clinical symptoms and laboratory results were collected, especially including white blood cell count, lymphocyte count, C-reactive protein (CRP).

Exclusion criteria were as follows: (1) patients accompanied with hypertension, diabetes, heart diseases, and any other pulmonary diseases; and (2) pregnant women. A total of 91 patients aged 20–50 years screened out of a public dataset of CT image involving 1000 confirmed COVID-19 patients were retrospectively analyzed and utilized as a deep learning validation set.

2.2 | Imaging protocol

The patients underwent the chest CT examination on a SOMATOM Definition AS+ 64-row scanner (Siemens Healthineers; Erlangen, Germany) and a uCT 530 40-row scanner (United Imaging Intelligence, China). The scanning parameters were set as follows: tube voltage = 120 kVp, automatic tube current modulation, matrix = 512 × 512, slice thickness = 5 mm, and spacing = 5 mm. The volumetric data with reconstructed 0.6–1-mm slice thickness were obtained for post-processing.

2.3 | Deep learning model

Two radiologists analyzed the CT images and collected the quantitative CT metrics. The assisted screening software for COVID-19 (United Imaging Intelligence, version R001, China) was utilized to screen lung lesions by VB-Net network and to segment lesion areas in lung window.[9,12] Figure 1 shows the interface and function of this software. The core algorithms of the system were described in detail in reference. The segmentation algorithm in the software employs a convolutional neural network framework,[10,11] which is an emerging and popular deep learning technology. Deep learning simulates the process of manual delineation of the infected regions, based on image features such as texture for GGO-like regions and consolidations. The algorithm automatically and implicitly learns these features, without any artificial processing. The software automatically segments, delineates, and paints the infected regions, just as a radiologist would manually do by using image

TABLE 1 Basic clinical and laboratory information

Basic information	Males ($n = 21$)	Females ($n = 28$)	Statistics	p Value
Age (years)	39.4 ± 7.1	42.1 ± 5.7	−1.461	0.151
Heart rate (bpm)	100.9 ± 15.1	98.1 ± 14.8	0.641	0.525
Respiratory rate (breaths/min)	21.0 ± 2.0	19.6 ± 3.2	1.864	0.069
PaO_2 (mmHg)	93.3 ± 3.9	96.9 ± 3.8	−3.24	**0.002**
Days from illness onset to admission	3.0 ± 1.3	5.4 ± 2.0	−4.748	**0.001**
Hospital stay	15.9 ± 7.9	14.6 ± 5.2	0.67	0.507
Severity				
Moderate cases	10 (47.6%)	19 (67.9%)	–	0.387
Severe cases	8 (38.1%)	7 (25.0%)		
Critical cases	3 (14.3%)	2 (7.1%)		
Signs and symptoms				
Fever	18 (85.7%)	21 (75.0%)	0.317	0.574
Cough	12 (57.1%)	19 (67.9%)	0.593	0.441
Fatigue	13 (61.9%)	9 (32.1%)	4.296	**0.038**
Headache	2 (9.5%)	4 (14.3%)	–	0.688
Myalgia	10 (47.6%)	7 (25.0%)	2.71	0.1
Sore throat	12 (57.1%)	10 (35.7%)	2.227	0.136
Laboratory findings				
Leucocytes	4.4 ± 1.7	3.9 ± 1.8	0.877	0.385
Normal (4–10×10^9/L)	10 (47.6%)	9 (32.1%)	1.211	0.376
Decreased	11 (52.4%)	19 (67.9%)		
Lymphocytes	1.39 ± 0.92	1.18 ± 0.67	0.902	0.372
Normal (1.1–3.2×10^9/L)	9 (42.9%)	13 (46.4%)	0.062	0.804
Decreased	12 (57.1%)	15 (53.6%)		
C-reactive protein	23.8 ± 20.0	21.6 ± 17.8	0.395	0.695
Normal (<10 mg/L)	7 (33.3%)	10 (35.7%)	0.030	0.862
Increased	14 (66.7%)	18 (64.3%)		

Note: Independent sample t test for continuous variables (mean ± SD), and χ^2 or Fisher exact test for categorical variables was used.
The signifiificance of using bold is that $p > 0.05$ for a significant difference.

FIGURE 1 An interface and the function of artificial intelligence–based software. The lesions are automatically delineated and segmented to calculate the infection volumes and percentages of infection in the whole lungs, lobes, bronchopulmonary segments, and even within a specific HU interval.

processing software. After segmentation, various indicators were calculated to quantify lung infections, including the volumes of infection in the entire lung, as well as each lobe and each bronchial lung segment. In addition, POI was calculated for the entire lung, each lobe, and bronchopulmonary segment to measure the severity of COVID-19 and the distribution of intra-pulmonary infections. The POI in three HU ranges (i.e., <−300, −300–49, and ≥50 HU representing GGO, mixed opacity, and consolidation) were also extracted.[10] ΔPOI was defined as the difference value of total POI in whole lungs between the second CT and initial CT scans. For clinical purpose, the principle of the AI system was not further illustrated in this study.

3 | STATISTICAL ANALYSIS

SPSS 13.0 software (IBM Corporation, Chicago, IL, USA) and GraphPad Prism 5.01 (GraphPad Software Inc., San Diego, CA) were used to perform statistical tests and plot bar charts. Kolmogorov–Smirnov test was used to assess the data distribution type. The numeric results are presented as the mean ± standard deviation (SD). Independent sample *t* test for continuous variables and χ^2 or Fisher exact test for categorical variables were used to compare the difference between the sexes. A multiple linear regression model was used to explore the values of initial total POI (iPOI), ΔPOI, and percentage of consolidation in predicting the hospital stay, after adjusting days from illness onset to admission, leucocytes, lymphocytes, CRP, age, and gender (male = 1 and female = 0). A p-value <0.05 was considered statistically significant. The POI of different lobes and lung segments was found to be skewed distributed, so the differences in POIs between groups were compared with Mann–Whitney *U* test, and the differences in POIs between three groups or above were compared using the Kruskal–Wallis *H* test.

4 | RESULTS

4.1 | Clinical and laboratory findings

The basic clinical and laboratory information were listed in Table 1. There were 21 men and 28 women included for analysis. All the patients had at least 2 CT scans, 14 patients had 4, and 29 had 3 for comparisons. Men had lower PaO_2 ($p = 0.002$) and shorter days from illness onset to admission ($p = 0.001$) than women. Men also had a longer hospital stay (15.9 ± 7.9 vs. 14.6 ± 5.2, $p = 0.507$) and a higher proportion of severe and critical cases than women (52.4% vs. 32.1%, $p = 0.387$). However, the results were insignificant. No significant difference was observed between two genders in age, heart rate, respiratory rate, fever, cough, headache, myalgia, and sore throat (all $p > 0.05$), except fatigue ($p = 0.038$). More than half of men and women showed decreased leucocytes and lymphocytes counts as well as increased CRP, but without significant difference between them.

TABLE 2 The correlations between computed tomography (CT) metrics, clinical, and laboratory indicators

Pearson coefficient	Hospital stay	Days from illness onset to admission	Leucocytes	Lymphocytes	CRP[a]	Age	Gender
Initial POI[b]	**0.666 (0.001)**	0.118 (0.209)	**−0.456 (0.001)**	**−0.398 (0.002)**	**0.573 (0.001)**	**0.276 (0.027)**	−0.029 (0.421)
ΔPOI	**0.704 (0.001)**	0.063 (0.332)	**−0.468 (0.001)**	**−0.435 (0.001)**	**0.608 (0.001)**	0.067 (0.325)	0.137 (0.175)
Consolidation	**0.726 (0.001)**	0.067 (0.324)	**−0.381 (0.003)**	**−0.437 (0.001)**	**0.594 (0.001)**	0.051 (0.363)	0.108 (0.229)

Note: The data presented were Pearson coefficient with *p* value in bracket. ΔPOI, the difference value of total POI in whole lungs between the second CT and initial CT scans.
[a]C-reactive protein.
[b]Percentage of infection.
The signifificance of using bold is that $p > 0.05$ for a significant difference.

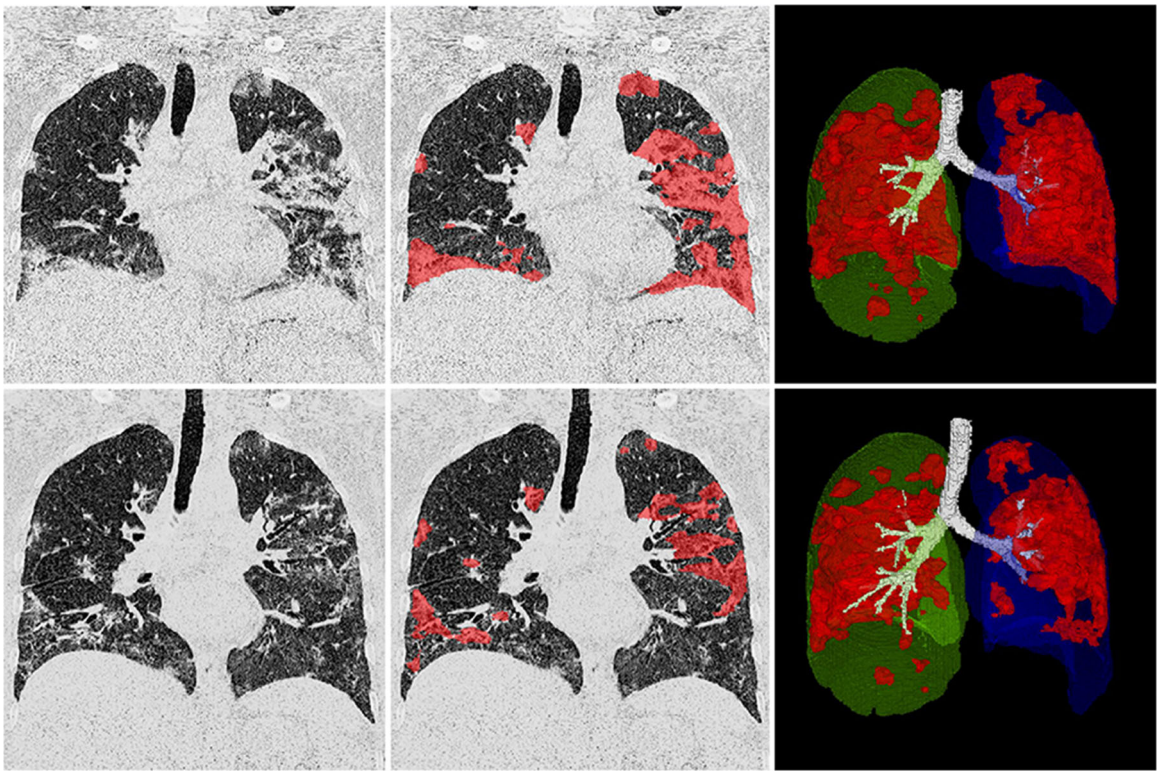

FIGURE 2 A coronavirus disease 2019 (COVID-19) patient with disease remission. Upper row and lower row showed initial and follow-up computed tomography (CT) with standard coronal image, coronal image with color covering the lesions and 3D surface rendering image. Initial CT images showed scattered consolidations with unclear edges and irregular shapes in bilateral lungs, especially in the left lower lobe. Most lesions were absorbed and the density decreased to ground-glass opacity and mixed opacity on follow-up CT. The 3D images provided a more stereoscopic vision for comparison.

4.2 | Artificial intelligence-based CT features

The correlations between CT metrics, clinical, and laboratory indicators were listed in Table 2. Figure 2 shows a COVID-19 patient with disease remission in a coronal and three-dimensional view with lesions highlighted. Figure 3 shows a COVID-19 patient with disease progression in the same view. The unstandardized B, standardized β, and collinearity statistics for each independent variable were listed in Table 3. Initial infection distribution in each lung lobe and bronchopulmonary segment in a total population, and in men and women were plotted in Figure 4a,b. Overall, right lower lobes had the highest POI, followed by left lower lobes, right upper lobes, middle lobes, and left upper lobes. The distributions of infections in lung lobes and bronchopulmonary segments were different between men and women. Men had higher POIs in entire lungs ($t = 2.105$, $p = 0.041$), left ($t = 2.291$, $p = 0.026$) and right upper lobes ($t = 2.521$, $p = 0.015$), and right middle lobes ($t = 2.231$, $p = 0.031$), but lower POIs in left

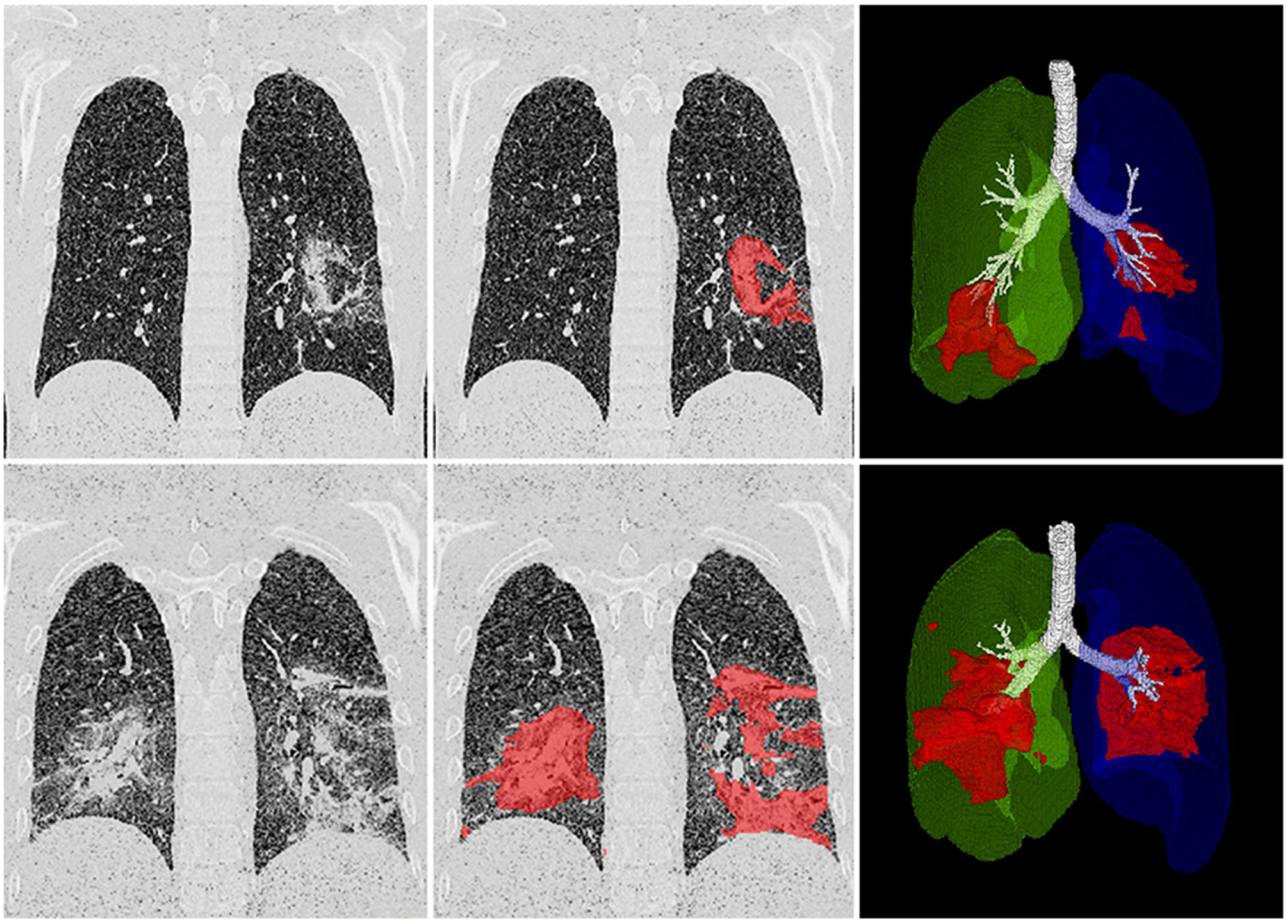

FIGURE 3 A coronavirus disease 2019 (COVID-19) patient with disease progression. Upper and lower rows show initial and follow-up computed tomography (CT) with standard coronal image, coronal image with color covering the lesions, and 3D surface rendering image. A regional lesion is observed in the dorsal segment of left lower lobe. Both consolidation and ground-glass opacity are automatically detected and labeled with red. The disease progress rapidly with a large area of consolidation in bilateral lower lobes observed. The lesion size in 3D image seems to be larger than that in coronal image.

TABLE 3 The unstandardized *B*, standardized *β*, and collinearity statistics for each independent variable

	Unstandardized *B*	Standardized *β*	*t*	*p*	Collinearity statistics	
					Tolerance	VIF[a]
Constant	9.8	–	3.195	0.003		
Initial POI[b]	0.129	0.212	2.703	**0.010**	0.576	1.735
ΔPOI	0.135	0.196	2.445	**0.019**	0.551	1.815
Consolidation	1.484	0.251	3.206	**0.003**	0.576	1.737
Days from illness onset to admission	−0.029	−0.009	−0.120	0.905	0.601	1.664
Leucocytes	−0.580	−0.015	−0.179	0.859	0.479	2.088
Lymphocytes	−1.607	−0.196	−2.209	**0.033**	0.450	2.220
CRP[c]	0.105	0.302	2.796	**0.008**	0.303	3.300
Age	0.015	0.015	0.219	0.828	0.723	1.383
Gender	0.81	0.063	0.817	0.419	0.588	1.700

Note: ΔPOI, the difference value of total POI in whole lungs between the second CT and initial CT scans.
The significance of using bold is that $p > 0.05$ for a significant difference.
[a]Variance inflation factor.
[b]Percentage of infection.
[c]C-reactive protein.

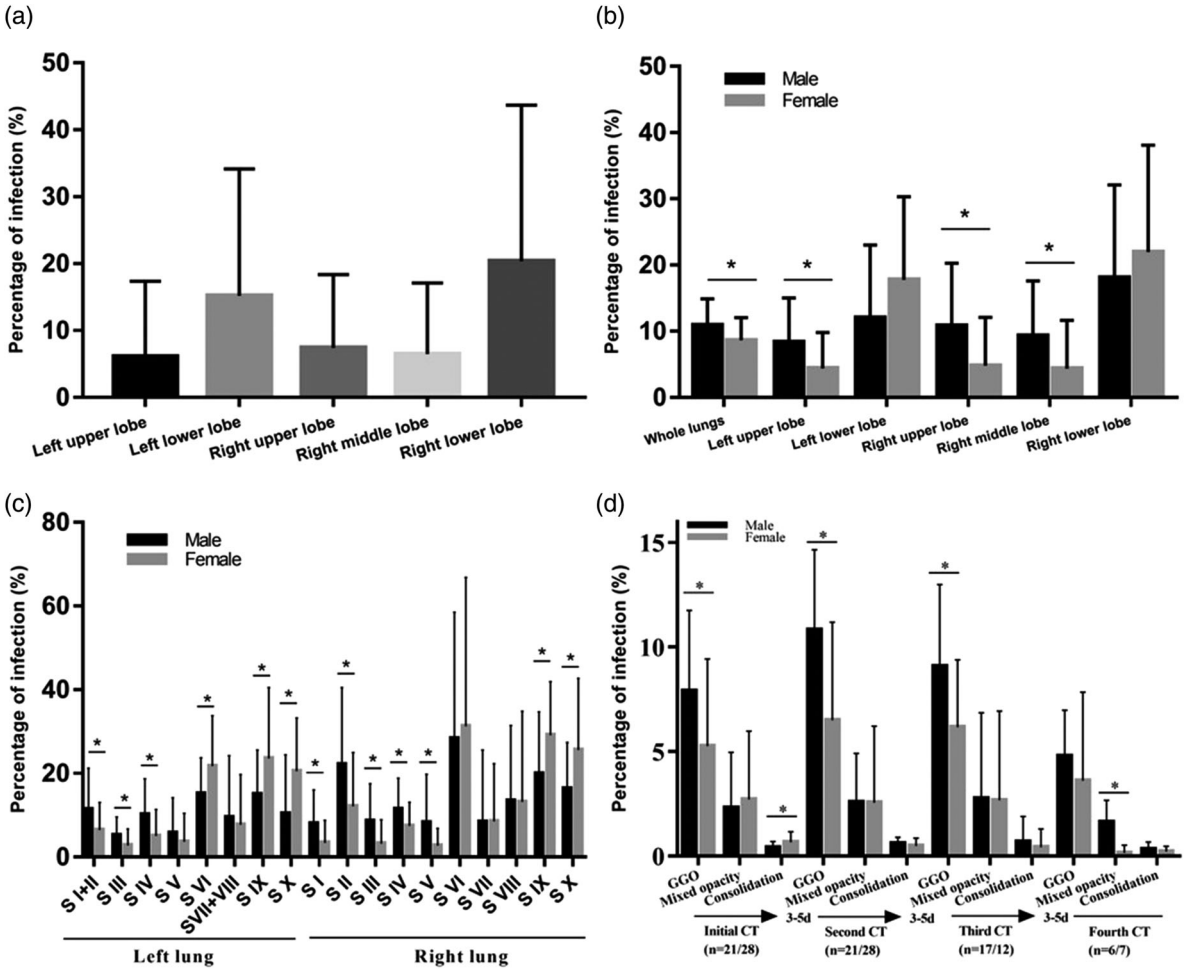

FIGURE 4 The percentages of three components on initial and follow-up computed tomographies (CTs) among men and women. (a) The overall percentage of infection (POI) in each lobe; (b) the POIs in each lobe among men and women; (c) the POIs in each bronchopulmonary segment among men and women; (d) multiple follow-up POIs in three specific HU regions among men and women. Independent sample *t* test was used. *$p < 0.05$. Left/right upper lobe: S I, apical segment; S II, posterior segment; S III, anterior segment; S I+II, apicoposterior segment. Left upper lobe: S IV, superior lingular segment; S V, inferior lingular segment. Right middle lobe: S IV, lateral segment; S V, medial segment. Left/right lower lobe: S VI, dorsal segment; S VII, medial basal segment; S VIII, anterior basal segment; S IX, lateral basal segment; S X, posterior basal segment; S VII+ VIII, anterior medial basal segment

($t = -1.669, p = 0.102$) and right lower lobes ($t = -0.879$, $p = 0.384$). Moreover, regarding the bronchopulmonary segment level, men had significantly higher POIs in apicoposterior segment ($t = 2.075$, $p = 0.044$), anterior segment ($t = 2.038$, $p = 0.047$), superior lingular segment ($t = 2.431$, $p = 0.019$), but lower POIs in dorsal segment ($t = -2.148$, $p = 0.037$), lateral basal segment ($t = -2.033$, $p = 0.048$), and posterior basal segment ($t = -2.639$, $p = 0.011$) of left lung. Higher POIs in apical segment ($t = 2.287, p = 0.029$), posterior segment ($t = 2.235$, $p = 0.030$), anterior segment ($t = 2.428$, $p = 0.021$), lateral segment ($t = 2.129$, $p = 0.039$), and medial segment ($t = 2.103, p = 0.046$), and lower POIs in lateral basal segment ($t = -2.333$, $p = 0.024$) and posterior basal segment ($t = -2.285$, $p = 0.027$) of right lung were also observed in men. These results indicated that the lesions were more likely to occur in or extend to bilateral upper lobes, superior lingular segment, and right middle lobes in men, which were more close to upper and front sides. The lesions in women were more concentrated in bilateral lower lobes, especially in dorsal segment, lateral basal segment, and posterior basal segment, which were more close to outer and back sides.

From the previous results, men showed a higher total POI and extensive infection, whereas women showed a less proportion but more intensive infection, prompting us that whether there existed a difference in the lesion density. After segmentation and quantitatively calculating the percentages of GGO, mixed opacity and consolidation based on CT values, men had a higher percentages of GGO ($t = 2.227$, $p = 0.031$), but less mixed opacity ($t = -0.465$, $p = 0.644$) and consolidation ($t = -2.113$, $p = 0.040$) than women in initial CT,

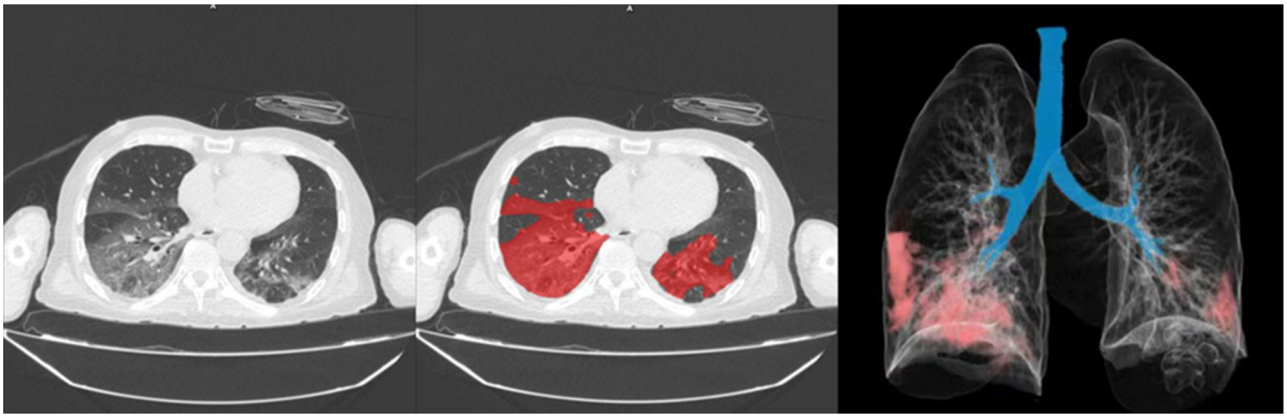

FIGURE 5 A coronavirus disease 2019 (COVID-19) patient from a public dataset.[17] It shows the areas of ground-glass opacity (GGO) in bilateral lower lung slices with a small amount of consolidation, including a large area of GGO in the right lower lung with reticular and/or interlobular septal thickening, and a small area of GGO in the left lower lung with consolidation. The red area covers the lesion, and the 3D image provides a more stereoscopic view for comparison. The lesion area of the right lung is significantly larger than that of the left lung.

conforming our hypothesis. From Figure 4d, we found that the percentage of GGO reached a peak on the second CT in both men and women, whereas the percentage of mixed opacity and consolidation maintained a high platform. Afterward, the components started to decrease, and obviously on the fourth CT. The distribution of lobe and bronchopulmonary segmental infections was different between males and females after an AI analysis of 91 patients, CT images in a public dataset. Figure 5 shows a moderate COVID-19 patient in an axial and three-dimensional view with lesions highlighted. Figure 6 shows a severe COVID-19 patient. Large areas of consolidation are observed in the bilateral lower lobes. The 3D image intuitively demonstrates multiple lesions with consolidations in the bilateral lungs. Figure 7 plots a mild COVID-19 patient. Extensive consolidation is shown in the right lower lung in the 3D image, whereas only a few lesions in the left lung.

The distribution of infections in the lung lobes and bronchopulmonary segments was different. In Figure 8, bar charts plot the distribution of infection in men and women in public dataset. At the lobar level, the POI levels of the whole lobe, right lobe, left lower lobe, and right lower lobe were significantly higher than those of the left lung, right upper lobe, right middle lobe, and left upper lobe. Additionally, the lesions in the both males and females were mainly located in the left and right lower lobes. However, the POI of the right upper lobe in the males was significantly higher than in the females ($Z = -2.371$, $p = 0.018$). At the level of lung segments, the lesions in both males and females were located mainly in the lateral base segment of the right lower lobe segment, the posterior basal segment of the right lower lobe, and the lateral basal segment of the left lower lobe. However, compared to the females, the POI in the males was significantly higher in the apical segment of the right upper lobe ($Z = -2.337$, $p = 0.019$), the posterior segment of the right upper lobe ($Z = -2.802$, $p = 0.005$), and the anterior segment of the right upper lobe ($Z = -2.183$, $p = 0.029$). Thus, the results of males in the 91 patients were consistent with those of the previous 49 patients in the bronchopulmonary segments of the right upper lobe.

After segmentation, the percentages of GGO, mixed opacityand consolidation based on CT values were quantitatively calculated. Among the 49 patients, the distribution of the lesions, including GGO ($t = 2.227$, $p = 0.031$), mixed opacity ($t = -0.465$, $p = 0.644$), consolidation ($t = -2.113$, $p = 0.040$), was significantly different between males and females. Comparatively, there were no significant differences in the distribution of GGO ($Z = -1.877$, $p = 0.061$), mixed opacity ($Z = -1.304$, $p = 0.192$), consolidation ($Z = -0.848$, $p = 0.396$)) between the 91 patients.

4.3 | CT metrics in regression model

In this part, we hypothesized that the duration of hospital stay could reflect the severity of illness and probably correlate with some of laboratory and imaging indicators. Therefore, a linear regression model was established and evaluated for the values of iPOI, ΔPOI, and percentage of consolidation in predicting the short-term outcome. The correlations between the three CT metrics and clinical as well as laboratory indicators were listed in Table 2. The unstandardized and standardized coefficients among each independent variable and dependent variable, as well as the collinearity statistics were listed in Table 3. Overall, $R = 0.928$ indicated a high model-fitting degree and adjusted $R^2 = 0.830$ suggested that all these independent variables collectively contributed the major variations in hospital stay. The Durbin–Watson coefficient was 1.984, which was close

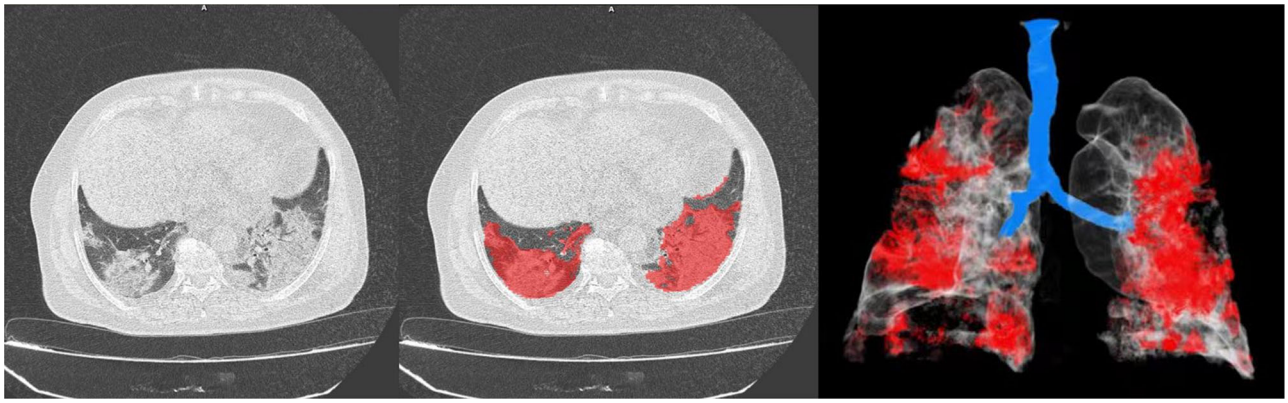

FIGURE 6 A severe coronavirus disease 2019 (COVID-19) patient from a public dataset. Large areas of consolidation are observed in the bilateral lower lobes. The 3D image intuitively shows that there are multiple consolidations in bilateral lungs.

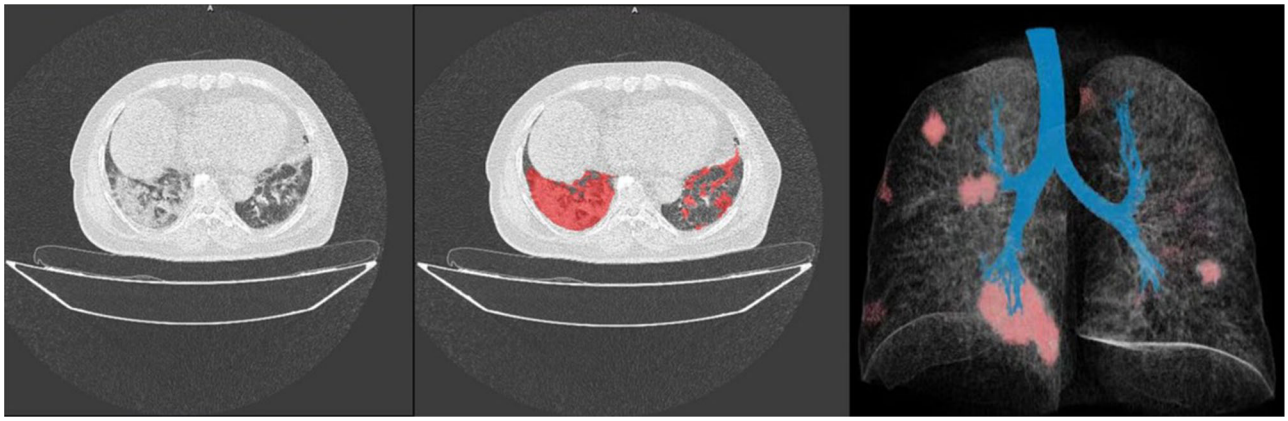

FIGURE 7 A mild coronavirus disease 2019 (COVID-19) patient from a public dataset.[17] A local consolidation in the lower right lung, and a small area of mixed opacity in the lower left lung. The extent of consolidation is shown in the right lower lung of the 3D image, a few lesions are shown in the left lung.

to 2. All the Tolerance coefficients were larger than 0.1 and variance inflation factors were less than 10, indicating that there was no multicollinearity among these independent variables. Their standardized β values were compared and suggested that CRP, percentage of consolidation, iPOI, ΔPOI, and lymphocyte counts degressively contributed to hospital stay.

The regression model can be expressed as hospital stay

$$\begin{aligned} &= 9.8 + 0.129 \times \text{iPOI} + 0.135 \times \Delta\text{POI} \\ &\quad + 1.484 \times \text{consolidation} - 1.607 \times \text{lymphocytes} \\ &\quad + 0.105 \times \text{CRP}. \end{aligned}$$

In this model, no correlation is found between days from illness onset to admission, leucocyte counts, age, gender, and hospital stays. The model indicates a larger POI and more consolidation components on initial CT, and an obvious increase of POI on follow-up CT will significantly prolong the duration of hospital stay. Besides, the iPOI, ΔPOI, and percentage of consolidation shows mild-to-moderate correlations with CRP, leucocytes, and lymphocyte counts (Pearson correlation coefficients ranged from 0.381 to 0.608, but less than 0.7).

5 | DISCUSSION

Currently, CT imaging plays an important role in screening COVID-19 and evaluating the severity of illness in the pandemic of viral pneumonia. A tool that can automatically quantify the lesions characteristics will significantly improve the work efficiency and diagnostic accuracy. Deep learning has become a promising technique in medical image analysis for feature extraction and successfully been applied to analyze diffuse interstitial lung disease[11] and differentiate viral and bacterial pneumonia on chest radiographs or CT images.[4,12] In this research, we used a deep learning–based software to segment and quantify the volume and percentage of COVID-19 infection on three-dimensional CT

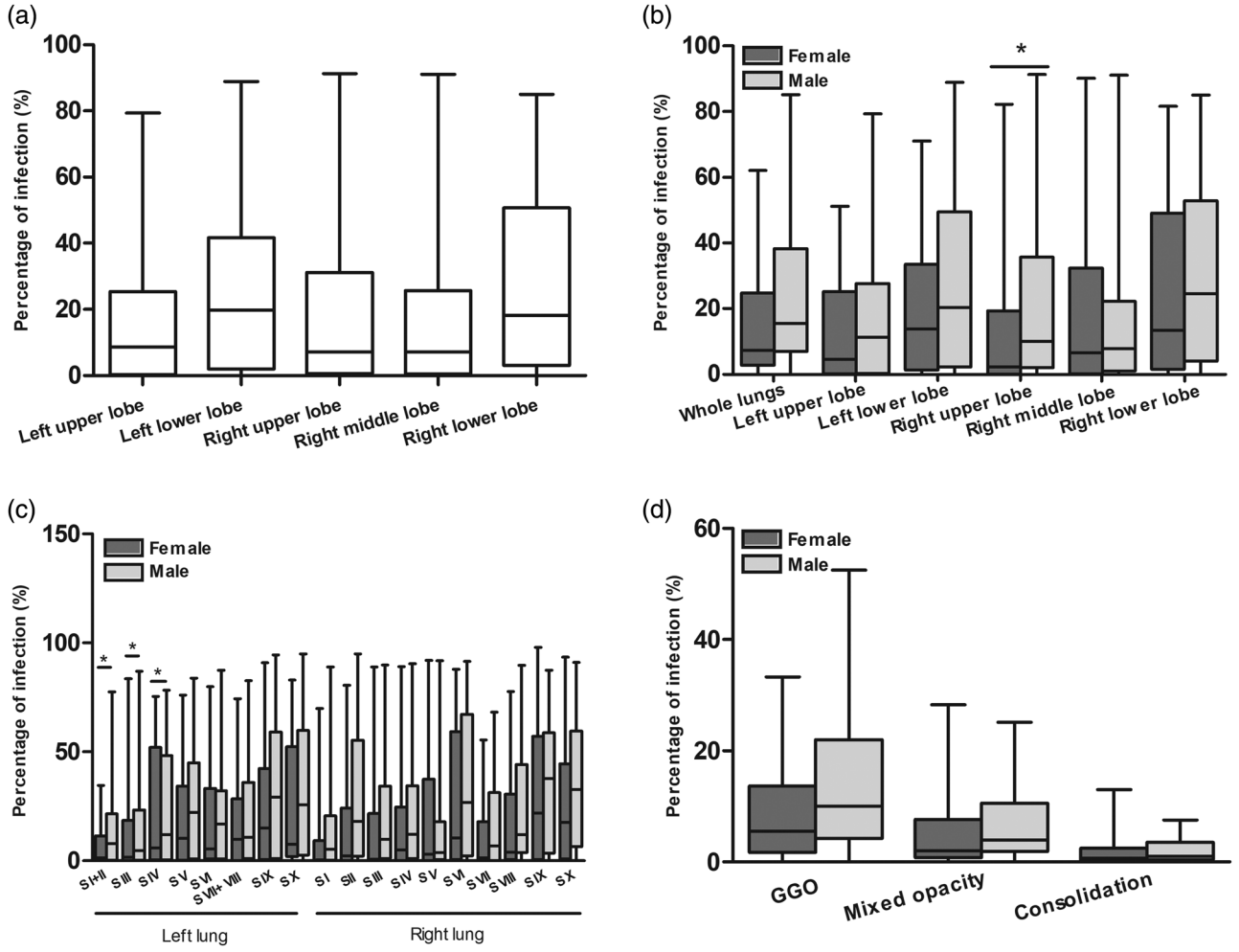

FIGURE 8 Bar charts plots the distribution of infection in men and women in public dataset:[17] (a) the overall percentage of infection (POI) in each lobe; (b) the POI of each lobe of the lung in both males and females; (c) the POI of each bronchopulmonary segment in both males and females; (d) the POI in three specific HU regions both male and female. Mann–Whitney *U* test $*p < 0.05$

volumetric images, which help us excavate more detailed information regarding lesion distribution, density, and the progress of each component on follow-up CT between male and female. The segmentation algorithm was tested in both a dataset of 49 patients and a public dataset of 91 patients. And the results of the AI segmentation were used for statistical analysis.

In this research, we found that men had a longer duration of hospital stay, higher proportion of severe and critical cases, and lower PaO_2 than women. Initial CT also suggested that men had a higher iPOI in entire lungs than women. Though only PaO_2 and iPOI showed statistical difference, they can still prompt that men may show a higher degree of severity when infected with SARS-CoV-2. A rapid progress was also observed in men regarding the shorter days from illness onset to admission and significantly higher ΔPOI (10.1% vs. 7.6%), compared with women. Many studies had reported the relationship between estrogen and immune system in antiviral response. One study had indicated that the diffuse alveolar damage in severe influenza was correlated with excessive inflammation, whereas estradiol was an effective anti-inflammatory hormone that relieved the severity of influenza A virus infection in women.[13] It can recruit more neutrophils to improve the reaction of influenza virus-specific CD8+ T cells for releasing more IFN-γ and TNF-α. They can promote virus elimination and improve the clinical outcome.[14] Another research also indicated that a higher level of testosterone may suppress their immune response and caused a higher morbidity of influenza in men.[15] Our study subdivided and quantified the contents of three components and tracked their follow-up changes, which may also reflect the dynamic process of pathology. GGO was a feature of alveolar edema and exudation of acute pulmonary injury, whereas consolidation suggested that the alveolus was completely filled with dense inflammatory exudation.[16] We found that men had more extensive and larger volume of GGO in bilateral lungs, whereas women showed less volume but denser lesions in

TABLE 4 Comparison of percentage of infection (POI) between male and female in public dataset

Category of lesions	Female POI (P50 [IQR])	Male POI (P50 [IQR])	*Z*	*p*
GGO[a]	5.5 (1.7,13.7)	10.1 (4.2,22.0)	−1.877	**0.061**
Mixed opacity	2.0 (0.8,7.7)	4.0 (1.9,10.6)	−1.304	0.192
Consolidation	0.7 (0.2,2.5)	1.1 (0.4,3.6)	−0.848	0.396

[a]Ground-glass opacity.
The signifificance of using bold is that $p > 0.05$ for a significant difference.

bilateral lower lobes. Estrogen may help the immune system detect and confront the virus in an early stage,[13] which could restrict the infection within the originally preferred regions. Regarding a larger percentage of consolidation in women on initial CT, the lesions may progress into a relatively late stage due to the longer days from illness onset to admission, compared to men. However, except for fatigue, the initial clinical symptoms were not showing difference between the sexes, indicating that this may not be the factor that influences the clinical outcome. The results of both groups showed that the lesions were located mainly in the lower lobes of both lungs. Specifically, the POI level of the right upper lobe in males was higher than that in females. For the 91 patients in the validation set, their lesions of GGO, the consolidation in males was not significantly different from those in females, which was inconsistent with the results of the 49 patients collected. The possible reason might lie in the relatively small sample size of the training set. The differences in mixed opacities between males and females were not significant in the 49 patients or the 91 patients, suggesting that males were consistent with females on the lesions of mixed opacities. Table 4 shows the POIs of three categories of lesions between the males and females in public dataset.[17]

Our research demonstrated the significant value of CT metrics in the effective management, disease grading, and prediction of clinical outcomes for patients with COVID-19. Some radiological indicators such as infection quality and POI, combined with other clinical data, have achieved good results in predicting disease severity and prognosis.

In the regression model, we incorporated iPOI and percentage of consolidation simultaneously into the model, considering that consolidation can reflect the severity of lesions in term of lesion density but only accounts for a small proportion in total infection. Change in percentage of consolidation will not obviously improve iPOI. Besides, no multiple collinearity was observed between any other two independent variables in this model. We found that the duration of hospital stay was positively correlated with iPOI, ΔPOI, percentage of consolidation and CRP, and negatively correlated with lymphocyte count. Guan et al.[18] had already reported that severe cases of COVID-19 showed significantly higher amounts of CRP than non-severe cases. A previous study showed that CT-based pulmonary inflammation index correlated with lymphocytes count, monocyte count, CRP, and procalcitonin, but correlation strengths were quite low with correlation coefficients ranging from 0.258 to 0.373 due to a semiquantitative value used.[16] In our study, a more precise quantifying technique was introduced, and the iPOI, ΔPOI, and percentage of consolidation showed higher correlations with leucocyte, lymphocyte counts, and CRP with the coefficients ranging from 0.381 to 0.608. Besides, the three CT metrics contributed the major variations (83%) in hospital stay combined with laboratory indicators. Although there are still a large number of people infected with COVID-19, proper supportive treatment also help reducing the duration of hospital stay in a certain extent and may account for the remaining part of variations in hospital stay.

There are several limitations in this research. First, the sample size is still small, which may lead to insignificant results regarding the severity of infection between the sexes, largely because we set strict inclusion criteria to maximally eliminate the influence of age and accompanied diseases and include the patients with more follow-up CT to track the dynamic changes of COVID-19. Second, the other laboratory indicators (e.g., neutrophil count, procalcitonin, and D-dimer) and imaging features (e.g., pleural effusion and lymphadenectasis) that may correlate with the clinical outcome were not investigated. Though the POIs within any HU intervals could precisely be extracted, the ideal threshold with the best diagnostic performance to distinguish GGO or mixed opacity from consolidation was still unclear.

6 | CONCLUSION

In this research, we used a more precise analyzing method to confirm the predilection of lesion distribution and severity of COVID-19 among men and women in a more homogeneous age group. Both men and women had characteristic distributions in lung lobes and bronchopulmonary segments. AI-based CT metrics can improve the recognition and quantification of GGO, mixed density and consolidation, and help the radiologists effectively and accurately determine the severity of the disease, compare the follow-up changes, and predict the outcome. At last, though men tend to demonstrate more serious infection than women, the results were insignificant, and more patients should be included for analysis in the future.

CONFLICT OF INTEREST

The authors have stated explicitly that there are no conflicts of interest in connection with this article.

ACKNOWLEDGMENTS

YXD is the guarantor of the paper and takes responsibility for the integrity of the work as a whole. YXD, ZSH, and LJY conceived the study; LWH, GJ, LJW, XF, LWS, and HXL acquired the data and authored the manuscript, performed data analysis and interpretation; LHH, ML, and ZFJ developed the artificial intelligence system. XCM provided some research site and equipment. All authors contributed substantially to the writing and review of the manuscript. We thank many teachers and friends for their good advice and kind help, who are Li Zhipeng, Haibo XU, Feng Xiao, Wang Yang, Shi Heshui, Han Xiaoyu, Chen Kuan, Chen Yu, and others. We thank all patients involved in the study.

REFERENCES

1. Ai T, Yang Z, Hou H, et al. Correlation of chest CT and RT-PCR testing in coronavirus disease 2019 (COVID-19) in China: a report of 1014 cases. *Radiology*. 2020;296:E32-E40.
2. Zu ZY, Jiang MD, Xu PP, et al. Coronavirus disease 2019 (COVID-19): a perspective from China. *Radiology*. 2020;296:E15-E25.
3. Xu X, Yu C, Qu J, et al. Imaging and clinical features of patients with 2019 novel coronavirus SARS-CoV-2. *Eur J Nucl Med Mol Imaging*. 2020;47:1275-1280.
4. Li L, Qin L, Xu Z, et al. Artificial intelligence distinguishes COVID-19 from community acquired pneumonia on chest CT. *Radiology*. 2020;(296):200905.
5. Li D, Wang D, Dong J, et al. False-negative results of real-time reverse-transcriptase polymerase chain reaction for severe acute respiratory syndrome coronavirus 2: role of deep-learning-based CT diagnosis and insights from two cases. *Korean J Radiol*. 2020;21(4):505-508.
6. Shan F, Gao Y, Wang J, et al. Lung infection quantification of COVID-19 in CT images with deep learning. 2020. https://arxiv.org/abs/2003.04655
7. Alghamdi IG, Hussain II, Almalki SS, Alghamdi MS, Alghamdi MM, El-Sheemy MA. The pattern of Middle East respiratory syndrome coronavirus in Saudi Arabia: a descriptive epidemiological analysis of data from the Saudi Ministry of Health. *Int J Gen Med*. 2014;7:417-423.
8. National Health Commission & State Administration of Traditional Chinese Medicine. Diagnosis and treatment protocol for novel coronavirus pneumonia (trial version 7). *Chin. Med. J*. 2020;133(09):1087-1095.
9. Mu G, Lin Z, Han M, Yao G, Gao Y. Segmentation of kidney tumor by multi-resolution VB-nets. 2019. [C]//2019 kidney Tumor Segmenttation Challenge:KiTS19.
10. Scholten ET, Jacobs C, van Ginneken B, et al. Detection and quantification of the solid component in pulmonary subsolid nodules by semiautomatic segmentation. *Eur Radiol*. 2015;25(2):488-496.
11. Park B, Park H, Lee SM, Seo JB, Kim N. Lung segmentation on HRCT and volumetric CT for diffuse interstitial lung disease using deep convolutional neural networks. *J Digit Imaging*. 2019;32(6):1019-1026.
12. Kermany DS, Goldbaum M, Cai W, et al. Identifying medical diagnoses and treatable diseases by image-based deep learning. *Cell*. 2018;172(5):1122-1131.e1129.
13. Vermillion MS, Ursin RL, Attreed SE, Klein SL. Estriol reduces pulmonary immune cell recruitment and inflammation to protect female mice from severe influenza. *Endocrinology*. 2018;159(9):3306-3320.
14. Robinson DP, Hall OJ, Nilles TL, Bream JH, Klein SL. 17beta-estradiol protects females against influenza by recruiting neutrophils and increasing virus-specific CD8 T cell responses in the lungs. *J Virol*. 2014;88(9):4711-4720.
15. Furman D, Hejblum BP, Simon N, et al. Systems analysis of sex differences reveals an immunosuppressive role for testosterone in the response to influenza vaccination. *Proc Natl Acad Sci USA*. 2014;111(2):869-874.
16. Wu J, Wu X, Zeng W, et al. Chest CT findings in patients with coronavirus disease 2019 and its relationship with clinical features. *Invest Radiol*. 2020;55(5):257-261.
17. Shakouri S, et al. COVID19-CT-dataset: an open-access chest CT image repository of 1000+ patients with confirmed COVID-19 diagnosis. *BMC Res. Notes*, 2021;14(1).

How to cite this article: Xudong Y, Weihong L, Feng X, et al. Artificial intelligence–based CT metrics used in predicting clinical outcome of COVID-19 in young and middle-aged adults. *Med Phys*. 2022;49:5604–5615.
https://doi.org/10.1002/mp.15803